Biophysical Journal, Volume *112*

Supplemental Information

Analysis of Active Transport by Fluorescence Recovery after Photobleaching

Maria-Veronica Ciocanel, Jill A. Kreiling, James A. Gagnon, Kimberly L. Mowry, and Björn Sandstede

Analysis of Active Transport by Fluorescence Recovery after Photobleaching - Supporting Material -

Maria-Veronica Ciocanel[a], Jill Kreiling[b], James Gagnon[c], Kimberly Mowry[b], Björn Sandstede[a,*]

[a] *Division of Applied Mathematics, Brown University, Providence, RI, United States*
[b] *Department of Molecular Biology, Cell Biology, and Biochemistry, Brown University, Providence, RI, United States*
[c] *Department of Molecular and Cellular Biology, Harvard University, Cambridge, MA, United States*
[*] *Corresponding author: bjorn_sandstede@brown.edu*

S1. Derivation of effective velocity and diffusion of transported particles for large times for a general model of intracellular transport. Examples: the 2-state and 4-state models

Consider particle dynamics that can be described by the following advection-reaction-diffusion equations:

$$\frac{\partial \boldsymbol{u}}{\partial t} = A\boldsymbol{u} + C\partial_y \boldsymbol{u} + D\partial_y^2 \boldsymbol{u}\,, \tag{1}$$

where $\boldsymbol{u}$ is an n-by-1 column vector of all populations of particles with different dynamic behavior, $A, C, D \in \mathbb{R}^{n\times n}$, with A the matrix of transition rates between the n states, C a diagonal matrix with real entries corresponding to velocities, and D a diagonal matrix with positive real entries for diffusion coefficients, respectively, of the n populations.

Taking the ansatz

$$(u_1, u_2, \ldots, u_n)^T(y,t) = e^{\lambda t}e^{\nu y}\tilde{\boldsymbol{u}}_{\boldsymbol{0}}\,, \tag{2}$$

with $\nu = ik$, equation (1) becomes:

$$(A + \nu C + \nu^2 D - \lambda I)\tilde{\boldsymbol{u}}_{\boldsymbol{0}} = 0\,. \tag{3}$$

Let $\boldsymbol{u_0}$ be the eigenvector of the zero eigenvalue of A, and $\boldsymbol{v}$ be in the generalized eigenspace $\mathscr{V}$ corresponding to all non-zero eigenvalues of A. Let $\boldsymbol{\psi_0}$ be the eigenvector corresponding to the zero eigenvalue of the adjoint matrix A^*.

Taking $\tilde{\boldsymbol{u}}_{\boldsymbol{0}} = a\boldsymbol{u_0} + \boldsymbol{v}$ allows us to apply a Lyapunov-Schmidt reduction to equation (3) by projecting it onto the $\mathscr{V}$ and $\boldsymbol{u_0}$ spaces.

1. Projection onto $\mathscr{V}$-space:

$$\text{eqn} - \frac{\langle \boldsymbol{\psi_0}, \text{eqn} \rangle}{\langle \boldsymbol{\psi_0}, \boldsymbol{u_0} \rangle} \boldsymbol{u_0}\,,$$

where eqn denotes equation (3). This gives:

$$\begin{aligned} a(A &+ \nu C + \nu^2 D - \lambda I)\boldsymbol{u_0} + (A + \nu C + \nu^2 D - \lambda I)\boldsymbol{v} \\ &- a\frac{\langle \boldsymbol{\psi_0}, (\nu C + \nu^2 D - \lambda I)\boldsymbol{u_0} \rangle}{\langle \boldsymbol{\psi_0}, \boldsymbol{u_0} \rangle}\boldsymbol{u_0} - \frac{\langle \boldsymbol{\psi_0}, (\nu C + \nu^2 D - \lambda I)\boldsymbol{v} \rangle}{\langle \boldsymbol{\psi_0}, \boldsymbol{u_0} \rangle}\boldsymbol{u_0} = 0\,. \end{aligned} \tag{4}$$

Note that $A\boldsymbol{u_0} = 0$ and $A^*\boldsymbol{\psi_0} = 0$ by definition, and $\langle \boldsymbol{\psi_0}, \lambda \boldsymbol{v} \rangle = \lambda \langle \boldsymbol{\psi_0}, \boldsymbol{v} \rangle = 0 \;\; \forall \boldsymbol{v} \in \mathscr{V}$.
It can also be shown for the fourth term in (4) that

$$\frac{\langle \boldsymbol{\psi_0}, (\nu C + \nu^2 D)\boldsymbol{v} \rangle}{\langle \boldsymbol{\psi_0}, \boldsymbol{u_0} \rangle} = \nu B_\nu \boldsymbol{v} \sim \mathscr{O}(\nu)$$

using the Cauchy-Schwartz inequality. Here B_ν is the operator sending $\boldsymbol{x} \to \frac{\langle \boldsymbol{\psi_0}, (C+\nu D)\boldsymbol{x} \rangle}{\langle \boldsymbol{\psi_0}, \boldsymbol{u_0} \rangle}$. Similarly, the third term in (4) is

$$a\frac{\langle \boldsymbol{\psi_0}, (\nu C + \nu^2 D - \lambda I)\boldsymbol{u_0} \rangle}{\langle \boldsymbol{\psi_0}, \boldsymbol{u_0} \rangle} = -a\lambda + a\nu B_\nu \boldsymbol{u_0} \sim -a\lambda + \mathscr{O}(\nu)\,.$$

Combining these observations yields:

$$a(\nu C + \nu^2 D - \cancel{\lambda I})\boldsymbol{u_0} + (A + \nu C + \nu^2 D - \lambda I - \nu \boldsymbol{u_0} B_\nu)\boldsymbol{v} + \cancel{a\lambda \boldsymbol{u_0}} - a\nu(B_\nu \boldsymbol{u_0})\boldsymbol{u_0} = 0\,.$$

Simplifying and separating $\boldsymbol{v}$ gives:

$$\begin{aligned} \boldsymbol{v} &= -a(A + \nu(C - \boldsymbol{u_0} B_\nu) + \nu^2 D - \lambda I)^{-1}(\nu C + \nu^2 D - \nu B_\nu \boldsymbol{u_0} I)\boldsymbol{u_0} \\ &\approx -a(\tilde{A}^{-1} + \mathscr{O}(\nu + \lambda))(\nu C - \nu B_\nu \boldsymbol{u_0} I + \nu^2 D)\boldsymbol{u_0} \\ &\approx -a\nu(\tilde{A}^{-1} + \mathscr{O}(\nu + \lambda)) \left(C - \frac{\langle \boldsymbol{\psi_0}, C\boldsymbol{u_0} \rangle}{\langle \boldsymbol{\psi_0}, \boldsymbol{u_0} \rangle} I + \mathscr{O}(\nu) \right) \boldsymbol{u_0}\,. \end{aligned} \tag{5}$$

Note that matrix $\tilde{A}$ corresponds to the projection of matrix A on space $\mathscr{V}$, so that $\tilde{A}$ is invertible. The inversion is allowed because the left-hand side ($\boldsymbol{v}$) is in the range of matrix A, and $\tilde{C}\boldsymbol{u_0} = \left(C - \frac{\langle \boldsymbol{\psi_0}, C\boldsymbol{u_0}\rangle}{\langle \boldsymbol{\psi_0}, \boldsymbol{u_0}\rangle} I\right)\boldsymbol{u_0}$ is also readily shown to be in the range of A.

2. Projection onto $\boldsymbol{u_0}$-space:

$$\langle \boldsymbol{\psi_0}, \text{eqn}\rangle\,,$$

where again eqn denotes equation (3)
Here, the projection gives:

$$\langle \boldsymbol{\psi_0}, (A + \nu C + \nu^2 D - \lambda I)(a\boldsymbol{u_0} + \boldsymbol{v})\rangle = 0\,.$$

Noting again that $A^*\boldsymbol{\psi_0} = 0$ and $\langle \boldsymbol{\psi_0}, \boldsymbol{v}\rangle = 0$, and using $\boldsymbol{v}$ from (5) results in:

$$\langle \boldsymbol{\psi_0}, (-\lambda I + \nu C + \nu^2 D - \nu^2(C + \nu D)\left[(\tilde{A}^{-1} + \mathscr{O}(\nu + \lambda))\left(C - \frac{\langle \boldsymbol{\psi_0}, C\boldsymbol{u_0}\rangle}{\langle \boldsymbol{\psi_0}, \boldsymbol{u_0}\rangle} I\right)\right]\boldsymbol{u_0}\rangle = 0\,. \tag{6}$$

Linearity of the inner product gives:

$$-\lambda\langle \psi_0, \boldsymbol{u_0}\rangle + \nu\langle \boldsymbol{\psi_0}, C\boldsymbol{u_0}\rangle + \nu^2\langle \boldsymbol{\psi_0}, D\boldsymbol{u_0}\rangle - \nu^2\langle \boldsymbol{\psi_0}, C\tilde{A}^{-1}\tilde{C}\boldsymbol{u_0}\rangle + \mathscr{O}(\nu^2(\nu+\lambda)) = 0\,.$$

Using the implicit function theorem and isolating $\lambda = \mathscr{O}(\nu)$, the higher order term at the end of the equation is $\mathscr{O}(\nu^3)$. Then λ is given by:

$$\boxed{\lambda = \nu\frac{\langle \boldsymbol{\psi_0}, C\boldsymbol{u_0}\rangle}{\langle \boldsymbol{\psi_0}, \boldsymbol{u_0}\rangle} + \nu^2\left[\frac{\langle \boldsymbol{\psi_0}, (D - C\tilde{A}^{-1}\tilde{C})\boldsymbol{u_0}\rangle}{\langle \boldsymbol{\psi_0}, \boldsymbol{u_0}\rangle}\right] + \mathscr{O}(\nu^3)\,.} \tag{7}$$

Returning to ansatz (2), component l of the vector of particle concentrations $\boldsymbol{u}$ is described by:

$$u_l(y,t) = e^{\left(a_1\nu + \frac{a_2}{2}\nu^2 + \sum_{j=3}^{\infty} a_j\nu^j\right)t} e^{\nu y}\tilde{u}_{0l}(y)\,, \tag{8}$$

where

$$\begin{aligned} a_1 &= \frac{\langle \boldsymbol{\psi_0}, C\boldsymbol{u_0}\rangle}{\langle \boldsymbol{\psi_0}, \boldsymbol{u_0}\rangle} \\ a_2 &= 2\frac{\langle \boldsymbol{\psi_0}, (D - C\tilde{A}^{-1}\tilde{C})\boldsymbol{u_0}\rangle}{\langle \boldsymbol{\psi_0}, \boldsymbol{u_0}\rangle}\,. \end{aligned}$$

Assuming a Dirac delta function initial condition $u_{0l} = \delta(y)$ (modeling a single particle located at $y = 0$), its Fourier transform in equation (8) is $\tilde{u}_{0l} = 1/(\sqrt{2\pi})$. Similar to the approach in [1], this allows us to calculate the concentration of particle population l by taking the inverse Fourier transform:

$$u_l = \frac{1}{\sqrt{2\pi}} \int_{-\infty}^{\infty} e^{ik(y+a_1 t) - \frac{a_2}{2}k^2 t} \times e^{\sum_{j=3}^{\infty} a_j \nu^j t} \times \frac{1}{\sqrt{2\pi}} dk \,.$$

As in [1], the change of variables $\tilde{y} = y + a_1 t$ and $\tilde{k} = kt^{1/2}$ gives:

$$u_l = \frac{1}{2\pi\sqrt{t}} \int_{-\infty}^{\infty} e^{i\tilde{k}\frac{\tilde{y}}{t^{1/2}} - \frac{a_2}{2}\tilde{k}^2} \times e^{\sum_{j=3}^{\infty} \frac{a_j (i\tilde{k})^j}{t^{j/2-1}}} d\tilde{k} \,.$$

In the second term in the product above, $j/2 - 1 > 0$, so that the summation vanishes as $t \to \infty$. It is therefore sufficient to calculate:

$$\begin{aligned} u_l &= \frac{1}{2\pi\sqrt{t}} \int_{-\infty}^{\infty} e^{i\tilde{k}\frac{\tilde{y}}{t^{1/2}} - \frac{a_2}{2}\tilde{k}^2} d\tilde{k} \\ &= \frac{1}{\sqrt{2\pi a_2 t}} e^{-\frac{(y+a_1 t)^2}{2a_2 t}} \,. \end{aligned}$$

Since this holds for each population l, the solution of the advection-reaction-diffusion PDEs for large time thus consists of a spreading Gaussian, and the effective velocity and diffusion of the particle behavior is given by:

$$\text{effective velocity} = a_1 = \frac{\langle \boldsymbol{\psi_0}, C\boldsymbol{u_0} \rangle}{\langle \boldsymbol{\psi_0}, \boldsymbol{u_0} \rangle} \tag{9}$$

$$\text{effective diffusion} = a_2 = 2\frac{\langle \boldsymbol{\psi_0}, (D - C\tilde{A}^{-1}\tilde{C})\boldsymbol{u_0} \rangle}{\langle \boldsymbol{\psi_0}, \boldsymbol{u_0} \rangle} \,. \tag{10}$$

We note that average transport velocity and spreading for the specific equations modeling neurofilament transport are derived in [1] and [2]. The spreading Gaussian solutions for large time have also been investigated for reaction-hyperbolic systems of PDEs in [3–6]. [7] introduces diffusion in the context of tug-of-war studies for motor-driven transport, with a focus on diffusion in one particle population. The approach outlined above provides analytical expressions for effective velocity and diffusion for large times for a system with arbitrary numbers of particles undergoing diffusion, bidirectional advection and reaction.

Effective velocity and diffusion for the 2-state model

We calculate the expressions for effective velocity and diffusion using the 2-state model of particle dynamics (see main text).

In this case, $C = \begin{pmatrix} c & \\ & 0 \end{pmatrix}$, $D = \begin{pmatrix} 0 & \\ & D \end{pmatrix}$ and $A = \begin{pmatrix} -\beta_1 & \beta_2 \\ \beta_1 & -\beta_2 \end{pmatrix}$.

The eigenvectors of A and A^* in equation (7) are given by $\boldsymbol{u_0} = \begin{pmatrix} \beta_2/(\beta_1+\beta_2) \\ \beta_1/(\beta_1+\beta_2) \end{pmatrix}$ and $\boldsymbol{\psi_0} = \begin{pmatrix} 1 \\ 1 \end{pmatrix}$.

This gives that the $\mathscr{O}(\nu)$ term in (7) is:

$$a_1 = \frac{\langle \boldsymbol{\psi_0}, C\boldsymbol{u_0} \rangle}{\langle \boldsymbol{\psi_0}, \boldsymbol{u_0} \rangle} = \frac{c\beta_2/(\beta_1+\beta_2)}{1} = \boxed{c\frac{\beta_2}{\beta_1+\beta_2}}, \tag{11}$$

which corresponds to the effective velocity in (9).

Similarly, the $\mathscr{O}(\nu^2)$ term in (7) is:

$$a_2 = 2\frac{\langle \boldsymbol{\psi_0}, (D - C\tilde{A}^{-1}\tilde{C})\boldsymbol{u_0} \rangle}{\langle \boldsymbol{\psi_0}, \boldsymbol{u_0} \rangle}.$$

Note that the non-zero eigenvalue of A is $\lambda_1 = -(\beta_1+\beta_2)$, and its corresponding eigenvector is $\boldsymbol{v} = (1,-1)^T$. Then $\tilde{A}\boldsymbol{v} = \lambda_1 \boldsymbol{v}$ and thus $\tilde{A}^{-1} = \lambda_1^{-1} = -\frac{1}{\beta_1+\beta_2}$.

Therefore:

$$\begin{aligned} a_2 = 2\frac{\langle \boldsymbol{\psi_0}, (D - C\tilde{A}^{-1}\tilde{C})\boldsymbol{u_0} \rangle}{\langle \boldsymbol{\psi_0}, \boldsymbol{u_0} \rangle} &= 2\frac{\langle \boldsymbol{\psi_0}, (D + (1/(\beta_1+\beta_2))C\tilde{C})\boldsymbol{u_0} \rangle}{1} \\ &= 2\langle \boldsymbol{\psi_0}, \left(D + \frac{1}{\beta_1+\beta_2} C \left(C - \frac{\langle \boldsymbol{\psi_0}, C\boldsymbol{u_0} \rangle}{\langle \boldsymbol{\psi_0}, \boldsymbol{u_0} \rangle} I \right) \right) \boldsymbol{u_0} \rangle \\ &= 2\langle \boldsymbol{\psi_0}, \left(D + \frac{1}{\beta_1+\beta_2} C \left(C - \frac{c\beta_2}{\beta_1+\beta_2} I \right) \right) \boldsymbol{u_0} \rangle \\ &= 2d\frac{\beta_1}{\beta_1+\beta_2} + 2c^2\frac{\beta_1\beta_2}{(\beta_1+\beta_2)^3}. \end{aligned}$$

Then

$$a_2 = \boxed{2d\frac{\beta_1}{\beta_1+\beta_2} + 2c^2\frac{\beta_1\beta_2}{(\beta_1+\beta_2)^3}}, \tag{12}$$

which corresponds to the expression for effective diffusion in (10).

[8] derive expressions similar to (11) and (12) for the effective speed and diffusion of an on/off transport particle using stochastic methods. Our analysis yields the additional first term in equation (12) compared to the expression for effective spread in [8], which is due to our assumption of diffusion in the off state.

Effective velocity and diffusion for the 4-state model

We also calculate the expressions for effective velocity and diffusion using the 4-state model of intracellular transport (see main text).

In this case, we have $C = \begin{pmatrix} c_+ & & & \\ & -c_- & & \\ & & 0 & \\ & & & 0 \end{pmatrix}$, $D = \begin{pmatrix} 0 & & & \\ & 0 & & \\ & & 0 & \\ & & & D \end{pmatrix}$, and transition rate matrix

$$A = \begin{pmatrix} -(\gamma_+ + \delta_+) & 0 & \alpha_+ & \beta_+ \\ 0 & -(\gamma_- + \delta_-) & \alpha_- & \beta_- \\ \delta_+ & \delta_- & -(\alpha_+ + \alpha_-) & 0 \\ \gamma_+ & \gamma_- & 0 & -(\beta_+ + \beta_-) \end{pmatrix}.$$

The eigenvectors of A and A^* in equation (7) can also be easily found: $\boldsymbol{\psi_0} = (1,1,1,1)^T$, and $\boldsymbol{u_0}$ corresponds to the proportions of each population at equilibrium (See Section S2). $\boldsymbol{u_0}$ can be normalized so that $\langle \boldsymbol{\psi_0}, \boldsymbol{u_0} \rangle = 0$.

This gives the $\mathscr{O}(\nu)$ term in (7):

$$\begin{aligned} \frac{\langle \boldsymbol{\psi_0}, C\boldsymbol{u_0} \rangle}{\langle \boldsymbol{\psi_0}, \boldsymbol{u_0} \rangle} &= -(\alpha_-\beta_-c_-\delta_+ + \alpha_-\beta_+c_-\delta_+ - \alpha_+\beta_-c_+\delta_- - \alpha_+\beta_+c_+\delta_- + \alpha_-\beta_-c_-\gamma_+ \\ &- \alpha_-\beta_+c_+\gamma_- + \alpha_+\beta_-c_-\gamma_+ - \alpha_+\beta_+c_+\gamma_+) \\ &/ \ (\alpha_-\beta_-\delta_+ + \alpha_+\beta_-\delta_- + \alpha_-\beta_+\delta_+ + \alpha_+\beta_+\delta_- + \alpha_-\beta_-\gamma_+ + \alpha_-\beta_+\gamma_- + \beta_-\delta_-\delta_+ \\ &+ \alpha_+\beta_-\gamma_+ + \alpha_+\beta_+\gamma_- + \beta_+\delta_-\delta_+ + \alpha_-\delta_+\gamma_- + \alpha_+\delta_-\gamma_+ + \beta_-\delta_-\gamma_+ + \beta_+\delta_+\gamma_- \\ &+ \alpha_-\gamma_-\gamma_+ + \alpha_+\gamma_-\gamma_+), \end{aligned} \tag{13}$$

which is the effective velocity in the 4-state example. Note that the above expression can be calculated using Matlab or Mathematica.

The $\mathscr{O}(\nu^2)$ term in equation (7) requires calculation of $a_2 = \frac{\langle \boldsymbol{\psi_0}, (D - C\tilde{A}^{-1}\tilde{C})\boldsymbol{u_0} \rangle}{\langle \boldsymbol{\psi_0}, \boldsymbol{u_0} \rangle}$. Noting that $R(A) = (R(\boldsymbol{\psi_0}))^\perp$, we seek a matrix representation of $\tilde{A}$ using

a basis in the complement of $\boldsymbol{\psi_0} = (1,1,1,1)^T$. A choice for this basis is $\boldsymbol{v_{01}} = (1,0,-1,0)^T$, $\boldsymbol{v_{02}} = (0,1,0,-1)^T$, and $\boldsymbol{v_{03}} = (1,0,0,-1)^T$, yielding:

$$\begin{aligned}
\tilde{A}\boldsymbol{v_{01}} &= \alpha_1\boldsymbol{v_{01}} + \alpha_2\boldsymbol{v_{02}} + \alpha_3\boldsymbol{v_{03}}\,, \\
\tilde{A}\boldsymbol{v_{02}} &= \beta_1\boldsymbol{v_{01}} + \beta_2\boldsymbol{v_{02}} + \beta_3\boldsymbol{v_{03}}\,, \\
\tilde{A}\boldsymbol{v_{03}} &= \gamma_1\boldsymbol{v_{01}} + \gamma_2\boldsymbol{v_{02}} + \gamma_3\boldsymbol{v_{03}}\,.
\end{aligned}$$

Note that α_i, β_i, γ_i have simple expressions that Matlab's or Mathematica's symbolic environments can readily find. This is done by solving equations of the form $V_0(\alpha_1,\alpha_2,\alpha_3)^T = \tilde{A}\boldsymbol{v_{01}}$, with $V_0 = (\boldsymbol{v_{01}},\boldsymbol{v_{02}},\boldsymbol{v_{03}})$.

Since we are interested in $\tilde{A}^{-1}\tilde{C}\boldsymbol{u_0}$, we seek $\bar{\boldsymbol{x}} = \bar{x}_1\boldsymbol{v_{01}} + \bar{x}_2\boldsymbol{v_{02}} + \bar{x}_3\boldsymbol{v_{03}}$ such that $\tilde{A}\bar{\boldsymbol{x}} = \tilde{C}\boldsymbol{u_0}$. Writing $\tilde{C}\boldsymbol{u_0} = \boldsymbol{x} = x_1\boldsymbol{v_{01}} + x_2\boldsymbol{v_{02}} + x_3\boldsymbol{v_{03}}$ gives:

$$\begin{aligned}
\alpha_1\bar{x}_1 + \beta_1\bar{x}_2 + \gamma_1\bar{x}_3 &= x_1\,, \\
\alpha_2\bar{x}_1 + \beta_2\bar{x}_2 + \gamma_2\bar{x}_3 &= x_2\,, \\
\alpha_3\bar{x}_1 + \beta_3\bar{x}_2 + \gamma_3\bar{x}_3 &= x_3\,.
\end{aligned}$$

Note that x_i can also be readily found for this example by solving $V_0(x_1,x_2,x_3)^T = \tilde{C}\boldsymbol{u_0}$ in Matlab. The equation for $\bar{x}_i$ is therefore:

$$\begin{pmatrix} \alpha_1 & \beta_1 & \gamma_1 \\ \alpha_2 & \beta_2 & \gamma_2 \\ \alpha_3 & \beta_3 & \gamma_3 \end{pmatrix} \begin{pmatrix} \bar{x}_1 \\ \bar{x}_2 \\ \bar{x}_3 \end{pmatrix} = \begin{pmatrix} x_1 \\ x_2 \\ x_3 \end{pmatrix}\,. \tag{14}$$

Given that α_i, β_i, γ_i and x_i have expressions that can be determined as described above, this linear system can be solved in Matlab or Mathematica. This recovers $\bar{\boldsymbol{x}} = \tilde{A}^{-1}\tilde{C}\boldsymbol{u_0} = \bar{x}_1\boldsymbol{v_{01}} + \bar{x}_2\boldsymbol{v_{02}} + \bar{x}_3\boldsymbol{v_{03}}$.

The $\mathscr{O}(\nu^2)$ term in the expression for λ is:

$$\begin{aligned}
a_2 = 2\frac{\langle\boldsymbol{\psi_0},(D - C\tilde{A}^{-1}\tilde{C})\boldsymbol{u_0}\rangle}{\langle\boldsymbol{\psi_0},\boldsymbol{u_0}\rangle} &= 2\frac{\langle\boldsymbol{\psi_0},(D - C\tilde{A}^{-1}\tilde{C})\boldsymbol{u_0}\rangle}{1} \\
&= 2\langle\boldsymbol{\psi_0}, D\boldsymbol{u_0} - C\bar{\boldsymbol{x}}\rangle \\
&= \boxed{2\boldsymbol{\psi_0}^T(D\boldsymbol{u_0} - C\bar{\boldsymbol{x}})\,.}
\end{aligned} \tag{15}$$

An analytical expression for this term can be found using the symbolic environments in Matlab or Mathematica.

S2. Calculation of percentages of particles in different states, and of expected run times and run lengths for cargo transported on microtubules

The equilibrium distributions of particles in different states given the general model (1) is readily obtained by solving

$$A\boldsymbol{u} = 0\,. \tag{16}$$

Then the additional assumption: $\sum_{i=1}^{n} u_i = 1$ yields the percentages of particles in each dynamic state at equilibrium.

An alternative approach to modeling particle mobility is by using a continuous-time Markov chain (CTMC) of the times and states of a particle undergoing intracellular transport. In this framework, we introduce matrix A with A_{ij} the rate of the transition from state i to state j, which corresponds to the transition matrix of the CTMC. Solving the linear system (16) becomes equivalent to solving the equilibrium or balance equations of the Markov process [9]. For the advection-diffusion 2-state model in the main text, the fractions of particles in each state are simply:

$$\text{fraction moving} \;=\; \frac{\beta_2}{\beta_1+\beta_2} \tag{17a}$$

$$\text{fraction diffusing} \;=\; \frac{\beta_1}{\beta_1+\beta_2}\,. \tag{17b}$$

The 4-state model expressions for fractions in each state are computed in a similar way and depend on all model transition rates.

The CTMC modeling approach is also useful in determining the dissociation-based quantities that appear in experimental literature, such as distances and times spent on microtubules before a motor-cargo complex unbinds [10]. It is well established that sojourn times of a homogeneous Markov chain in each state i are exponentially distributed with parameter q_i, where q_i is the transition rate of leaving state i for any other state [9]. This means that the mean sojourn times for the 2-state model are:

$$\text{expected run time} \;=\; \frac{1}{\beta_1}\,,$$

$$\text{expected run length} \;=\; \frac{1}{\beta_2}\,.$$

Similarly, the mean times in the states of the 4-state model are given by:

$$\begin{aligned}
\text{expected run time up} &= \frac{1}{\gamma_- + \delta_-}\,, &&\text{expected time diffusing} &= \frac{1}{\beta_- + \beta_+}\,,\\
\text{expected run time down} &= \frac{1}{\gamma_+ + \delta_+}\,, &&\text{expected time pausing} &= \frac{1}{\alpha_- + \alpha_+}\,.
\end{aligned}$$

The expected run length of motor-cargo complexes on microtubule filaments is then simply the speed in the desired direction times the mean sojourn time in the corresponding moving state. For the 4-state model, this yields:

$$\begin{aligned}
\text{expected run length up} &= \frac{c_-}{\gamma_- + \delta_-}\,,\\
\text{expected run length down} &= \frac{c_+}{\gamma_+ + \delta_+}\,.
\end{aligned}$$

S3. Supplementary Figures and Tables

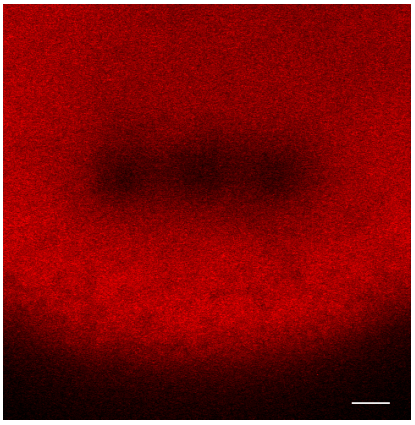

Figure 1: Shown is a representative oocyte in which three 5 μm circular ROIs of βG-MS2 RNA (β-globin RNA) bound by MCP-mCh were bleached as detailed in the main text. Scale bar corresponds to 10 μm. Note that Figure 4B in the main text shows a sample postbleach intensity profile extracted from a similar image. That profile is then used as an initial condition for the numerical parameter estimation.

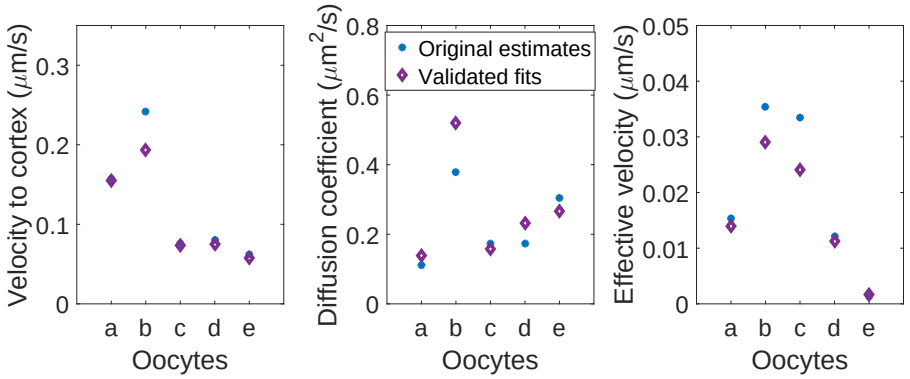

Figure 2: Parameter estimates from Region 1 VLE RNA FRAP data for individual oocyte trials are validated using PDE-generated FRAP recovery curves (5 trials shown).

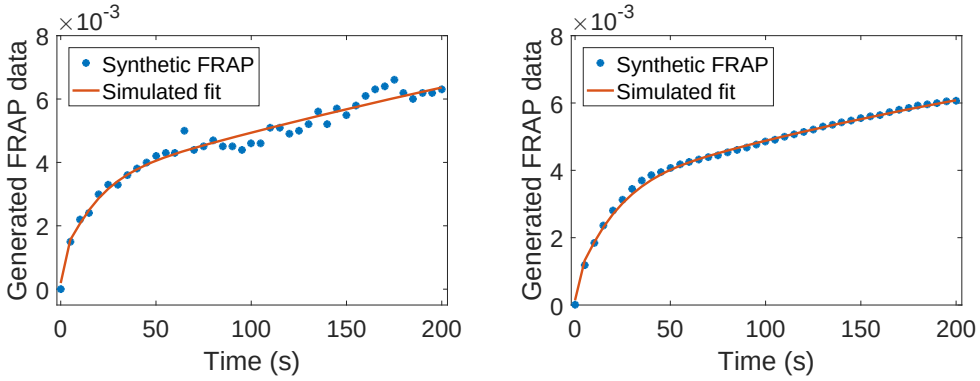

Figure 3: Sample synthetic data generated using the Markov Chain approach (10^4, respectively 10^6 RNAs) based on the 4-state model are fit using our parameter estimation procedure. The synthetic data on the left is not smooth since this stochastic model for data generation creates realistic noisy FRAP recovery curves. We note that the approximately 10^8 RNAs injected in the oocytes correspond to roughly 10^4-10^6 RNAs given the spatial domain considered in our simulations.

Table 1: Table of input and output parameters for Figure 3. Input corresponds to parameters used for data generation, Output (10^4) corresponds to parameters estimated using data generated with 10^4 RNAs, and Output (10^6) corresponds to parameters estimated using data generated with 10^6 RNAs.

	c_+ $(\mu m/s)$	c_- $(\mu m/s)$	d $(\mu m^2 s^{-1})$	α_+ (s^{-1})	α_- (s^{-1})	δ_+ (s^{-1})	δ_- (s^{-1})
Input	0.157	2e−4	0.11	0.008	4e−6	3e−4	0.12
Output (10^4)	0.114	2e−6	0.05	0.002	0.005	0.03	0.08
Output (10^6)	0.13	3e−5	0.09	3e−5	0.008	0.03	0.05

Table 2: Estimated parameters for FRAP WT average data based on 5 oocytes using the 2-state model for VLE RNA. While the estimates for speed c and diffusion coefficient d are provided in the main text as well for this set, here we also include the estimates of reaction rates β_1 and β_2.

Region	c $(\mu m/s)$	d $(\mu m^2 s^{-1})$	β_1 (s^{-1})	β_2 (s^{-1})
1	0.05	0.26	2.3e−14	0.006
2	0.09	1.42	0.003	0.0007
3	0.07	0.83	4e−5	1.4e−6

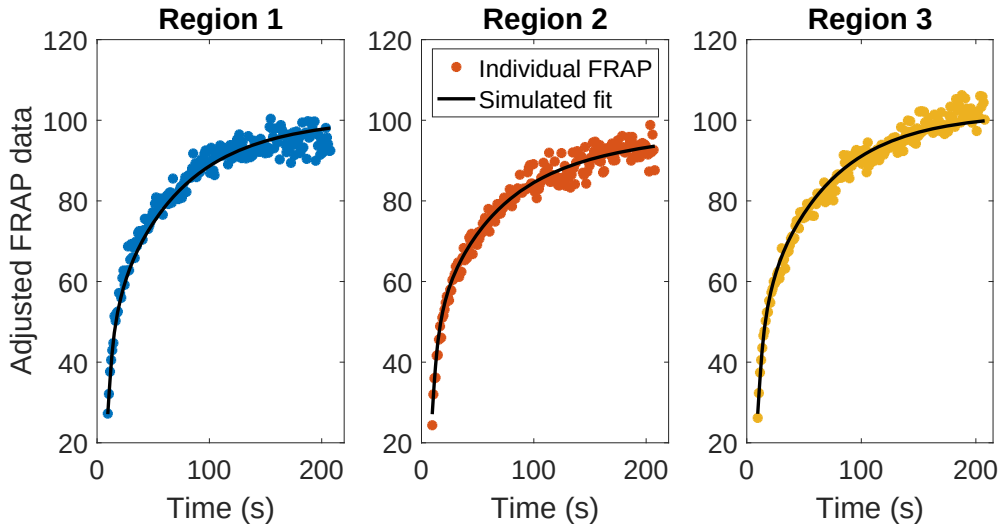

Figure 4: Sample oocyte β-globin RNA FRAP data for all 3 regions is fit using our parameter estimation procedure. Note that the same estimated parameters generate fits to data from all 3 bleach spots in the initial condition (see Figure 1). Estimated parameters are $D = 2.77\ \mu m^2/s$, $\beta_1 = 0.03\ s^{-1}$ and $\beta_2 = 0.05\ s^{-1}$.

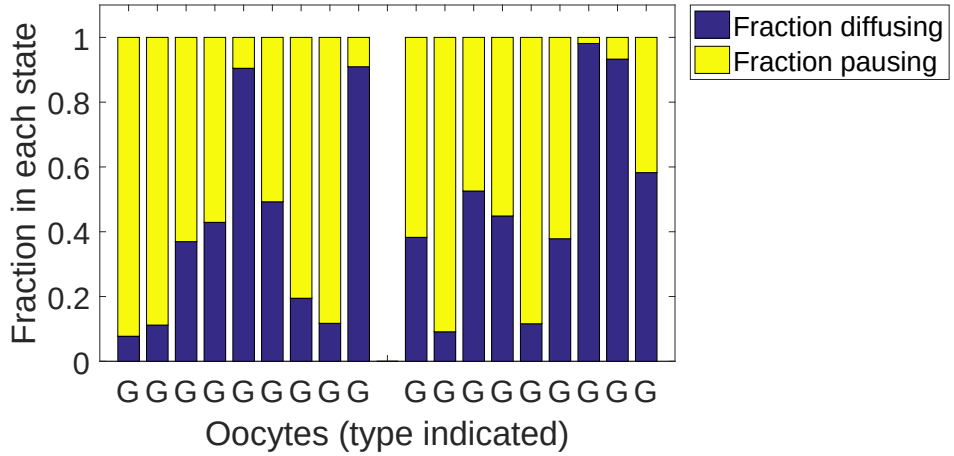

Figure 5: Predicted fractions of nonlocalizing β-globin RNA (G) in diffusing and stationary states for two additional sets of 9 healthy oocytes each (individual oocyte trials). The sets provided here and in the main text are each from FRAP experiments carried out on different days. The average diffusion coefficient d for the first set is 1.8 $\mu m^2/s$ (with standard deviation 1.1 $\mu m^2/s$), and for the second set 3.1 $\mu m^2/s$ (with standard deviation 1.5 $\mu m^2/s$). mRNA particles are predicted to spend on average 60% of time in a paused state (with standard deviation 32%) for the first set, and 51% of time (with standard deviation 31%) for the second set. Parameter estimation is set up with a three bleach spot initial condition for β-globin RNA (see Figure 4B in the main text).

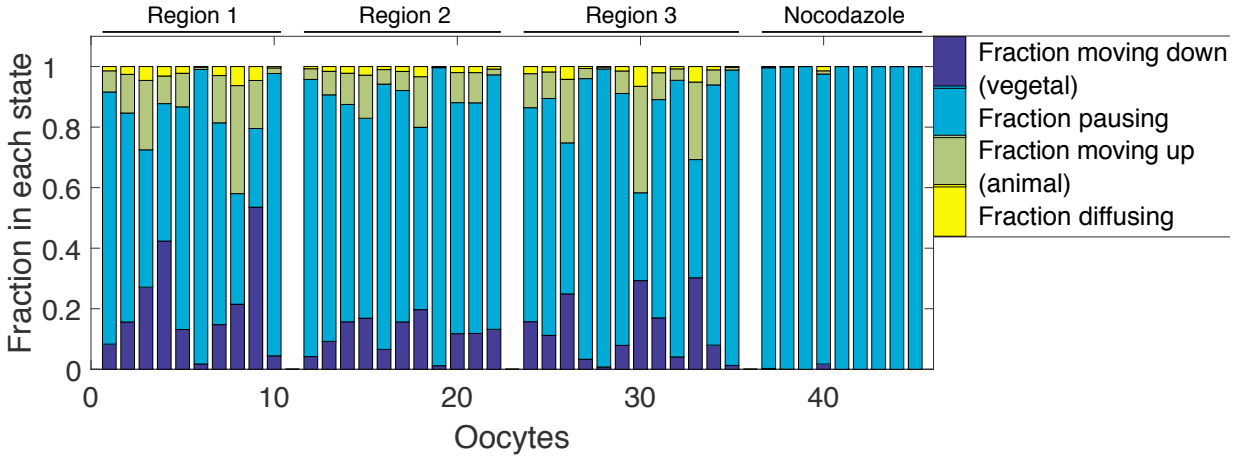

Figure 6: Predicted fractions of localizing VLE RNA in different states for individual oocyte trials in healthy and Nocodazole-treated (N) oocytes. The fits are carried out using the 4-state model.

S4. Adjusted FRAP data

The procedure for adjusting the raw FRAP data to correct for photofading during image acquisition is outlined in [11]. We provide the details here for completion.

We refer to the raw time series fluorescence data for each photobleached region of interest in the vegetal cytoplasm of *Xenopus* oocytes as $\mathrm{ROI}(t)$. Additional measurements available from FRAP experiments are the fluorescence data from the non-photobleached regions outside and inside the oocyte at time t, which we denote by $\mathrm{ROI}_o(t)$ and $\mathrm{ROI}_n(t)$, respectively. To correct the raw FRAP data for acquisition photobleaching, we calculate the adjusted fluorescence time series $A(t)$ as

$$A(t) = F(t) \times \frac{F_{\mathrm{pre}}}{F_{\mathrm{n}(t)}} = (\mathrm{ROI}(t) - \mathrm{ROI}_o(t)) \times \frac{(\mathrm{ROI}_n(1) - \mathrm{ROI}_o(1))}{(\mathrm{ROI}_n(t) - \mathrm{ROI}_o(t))}\,. \quad (18)$$

Here the background subtracted fluorescence at time t is denoted by $F(t)$, the background subtracted average intensity for all prebleach frames is denoted by F_{pre}, and $F_n(t)$ denotes the background subtracted fluorescence intensity value in a neighboring region at time t. It is worth noting the meaning of the second equality in equation (18): to obtain $F(t)$, we subtract the background fluorescence $\mathrm{ROI}_o(t)$ from the fluorescence intensity in the region of interest $\mathrm{ROI}(t)$; to obtain F_{pre}, we subtract the background fluorescence of the prebleach frames $\mathrm{ROI}_o(1)$ from prebleach fluorescence outside the cortical region $\mathrm{ROI}_n(1)$; and to yield $F_n(t)$, we subtract the background fluorescence intensity $\mathrm{ROI}_o(t)$ from the fluorescence at the neighboring region outside the cortical region $\mathrm{ROI}_n(t)$.

S5. Numerical Methods

Numerical integration of equations of the form (1) is done using exponential time-differencing Runge-Kutta methods [12, 13] coupled with space discretization using Fourier spectral methods. The boundary conditions for the PDE systems are taken to be periodic in both the x and y dimensions. The spatial domain size is taken to be large relative to the bleach spot size, with length scales of 40 μm in the horizontal direction x, and 60 μm in the vertical direction of movement y. We used 64 Fourier modes in the spectral decomposition in both directions, which is sufficient for the purpose of our simulations. Finally, different time steps were tested, and $\Delta t = 0.1$ was chosen for yielding consistent results while also minimizing computation costs.

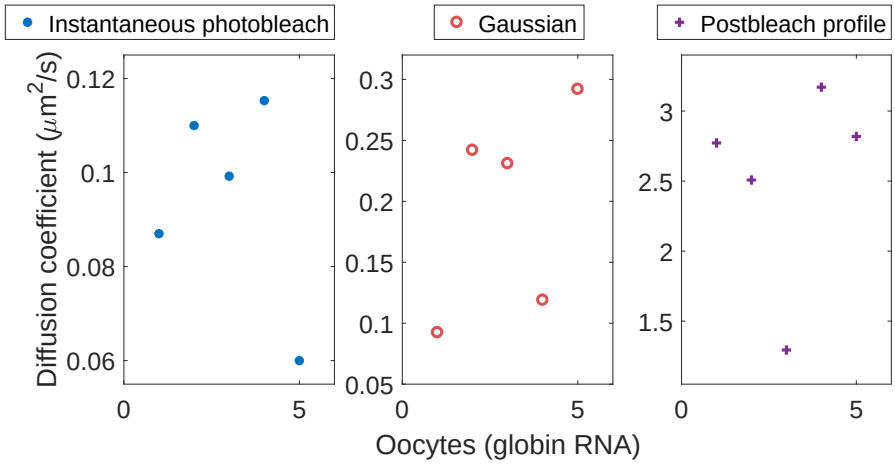

Figure 7: Estimated diffusion coefficients for β-globin RNA using the same set of 5 oocytes with instantaneous photobleach (flat circular disk initial conditions), Gaussian initial conditions, and the experimental photobleach profile (exponential of Gaussian initial condition), left to right. Note the different scales of the vertical axis.

Matlab code for generating synthetic data and for performing parameter sweeps and estimation is included in the *S5_Matlab_code_FRAP.zip* file.

S6. Accounting for the dynamics during the FRAP photobleach process: Supporting figures

Section 3.5 in the main text outlines the importance of accounting for the dynamics occurring during the photobleach process when modeling the initial condition for our numerical FRAP parameter estimation methods. Figure 7 shows the sensitivity of the diffusion coefficient estimates for the same set of 5 oocytes to the initial condition (flat circular disk, Gaussian, or exponential of Gaussian initial condition). In Figure 8 we include additional diffusion coefficient estimates for β-globin RNA using the instantaneous bleaching and photobleach profile (exponential of Gaussian) initial conditions. In addition, we also include estimates of diffusion coefficients for a set of 7 oocytes and speed in the animal pole direction in region 3 (c_-) for a set of 5 oocytes using both settings.

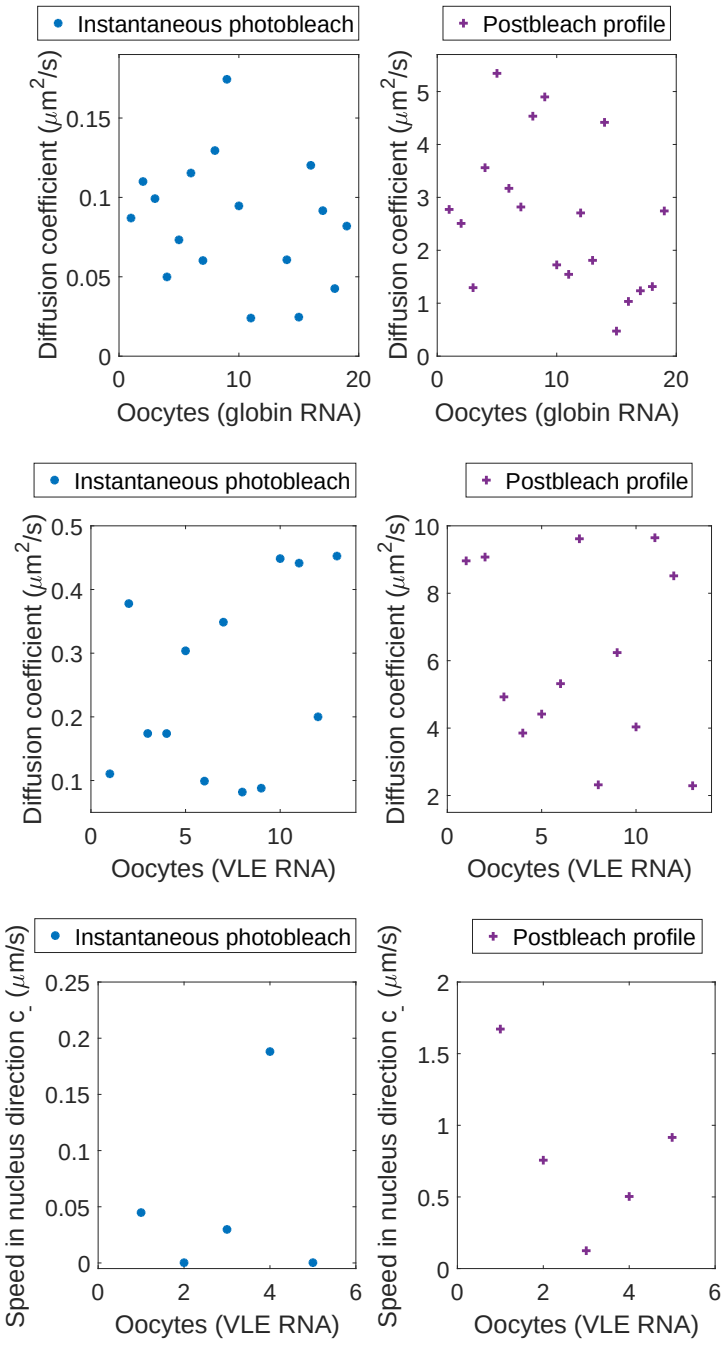

Figure 8: Estimated diffusion coefficients for β-globin RNA, diffusion coefficient for VLE RNA, and speed in the animal pole direction in region 3 for VLE RNA using the instantaneous photobleach and experimental photobleach profile initial conditions (top to bottom).

Supporting References

[1] P. Jung, A. Brown, Modeling the slowing of neurofilament transport along the mouse sciatic nerve, Physical Biology 6 (4) (2009) 046002.

[2] Y. Li, A. Brown, P. Jung, Deciphering the axonal transport kinetics of neurofilaments using the fluorescence photo-activation pulse-escape method, BMC Neuroscience 15 (Suppl 1) (2014) P132.

[3] M. C. Reed, S. Venakides, J. J. Blum, Approximate traveling waves in linear reaction-hyperbolic equations, SIAM Journal on Applied Mathematics 50 (1) (1990) 167–180.

[4] A. Friedman, G. Craciun, Approximate traveling waves in linear reaction-hyperbolic equations, SIAM journal on mathematical analysis 38 (3) (2006) 741–758.

[5] A. Friedman, H. BEI, Uniform convergence for approximate traveling waves in linear reaction-hyperbolic systems, Indiana University Mathematics journal 56 (5) (2007) 2133–2158.

[6] J. M. Newby, P. C. Bressloff, Quasi-steady state reduction of molecular motor-based models of directed intermittent search, Bulletin of mathematical biology 72 (7) (2010) 1840–1866.

[7] J. Newby, P. C. Bressloff, Random intermittent search and the tug-of-war model of motor-driven transport, Journal of Statistical Mechanics: Theory and Experiment 2010 (04) (2010) P04014.

[8] L. Popovic, S. A. McKinley, M. C. Reed, A stochastic compartmental model for fast axonal transport, SIAM Journal on Applied Mathematics 71 (4) (2011) 1531–1556.

[9] F. Beichelt, Stochastic processes in science, engineering and finance, CRC Press, 2006.

[10] J. Hughes, W. O. Hancock, J. Fricks, Kinesins with extended neck linkers: a chemomechanical model for variable-length stepping, Bulletin of mathematical biology 74 (5) (2012) 1066–1097.

[11] E. A. Powrie, V. Ciocanel, J. A. Kreiling, J. A. Gagnon, B. Sandstede, K. L. Mowry, Using in vivo imaging to measure rna mobility in xenopus laevis oocytes, Methods.

[12] S. Cox, P. Matthews, Exponential time differencing for stiff systems, Journal of Computational Physics 176 (2) (2002) 430–455.

[13] A.-K. Kassam, L. Trefethen, Fourth-order time-stepping for stiff PDE's, SIAM Journal on Scientific Computing 26 (4) (2005) 1214–1233.